Materials Research Bulletin 129 (2020) 110887

Contents lists available at ScienceDirect

Materials Research Bulletin

journal homepage: www.elsevier.com/locate/matresbu

Improved microwave dielectric properties of novel low-permittivity Sn-doped $Ca_2HfSi_4O_{12}$ ceramics

Kang Du[a,b], Xiao-Qiang Song[a,b], Zheng-Yu Zou[a,b], Jun Fan[a,b], Wen-Zhong Lu[a,b], Wen Lei[a,b,*]

[a] School of Optical and Electronic Information, Huazhong University of Science and Technology, Wuhan, 430074, PR China
[b] Key Lab of Functional Materials for Electronic Information (B), Ministry of Education, Wuhan, 430074, PR China

ARTICLE INFO

Keywords:
$Ca_2HfSi_4O_{12}$ ceramic
Sn^{4+} substitution for Hf^{4+}
Phase composition
Microwave dielectric properties

ABSTRACT

The phase compositions and microwave dielectric properties of $Ca_2(Hf_{1-x}Sn_x)Si_4O_{12}$ ($0 \le x \le 0.5$) were investigated by the solid-state reaction method. A single-phase ceramic with monoclinic structure was formed in the $Ca_2(Hf_{1-x}Sn_x)Si_4O_{12}$ ($0 \le x \le 0.2$) ceramic. At $0.25 \le x \le 0.5$, $CaSiO_3$ and $CaSnSiO_5$ second phases appeared. The microwave dielectric properties of a novel $Ca_2HfSi_4O_{12}$ ceramic ($\varepsilon_r = 8.1$, $Q\times f = 39{,}700$ GHz and $\tau_f = -12.7$ ppm/°C) were obtained. Partial substitution of Sn^{4+} for Hf^{4+} could reduce its relative permittivity and improve quality factor, and the highest quality factor of 49,500 GHz was obtained at $x = 0.2$. The τ_f value of $Ca_2(Hf_{1-x}Sn_x)Si_4O_{12}$ ceramics could be controlled to a near-zero value by the $CaSnSiO_5$ second phase when $x > 0.3$. The optimum microwave dielectric properties ($\varepsilon_r = 8.0$, $Q\times f = 37{,}100$ GHz and $\tau_f = -7.2$ ppm/°C) were achieved in the $Ca_2(Hf_{1-x}Sn_x)Si_4O_{12}$ ($x = 0.4$) ceramic.

1. Introduction

With the fast development of 5 G mobile, microwave communication technology and driverless technology, the demands for microwave dielectric components and materials are gradually increasing. The use of microwave dielectric ceramics with low permittivity ($\varepsilon_r < 15$), high quality factor ($Q\times f$) and near-zero temperature coefficient of resonant frequency (τ_f) has been increasing rapidly in the last decade [1–6]. The characteristic of low permittivity can improve signal propagation speed among conductors. High $Q\times f$ and near-zero τ_f values are also necessary for microwave dielectric components because they can improve the frequency selectivity and stability against temperature, respectively.

Silicates have attracted considerable attention due to their low ε_r and high $Q\times f$ values. Table 1 shows many types of silicates with low ε_r and high $Q\times f$ value, which exhibit a low ε_r value due to a large number of Si–O bonds in [SiO_4] tetrahedra. The high content of covalent bond (55 %) in the Si–O bond can decrease ε_r value because of the reduction in the rattling effect [16]. Therefore, silicates with a low permittivity and a high $Q\times f$ value are suitable as dielectric materials for high-frequency devices. However, according to the ε_r–τ_f relationship [17,18], silicates possess a generally high-magnitude negative τ_f value. $Ca_3(Zr_{1-x}Sn_x)Si_2O_9$ ceramics show low-permittivity microwave dielectric properties and a stable crystal structure with the [Si_2O_7] group, [$Zr_{1-x}Sn_xO_6$] and [$CaO_{6/7}$] polyhedron [12]. The τ_f value of $Ca_3Sn_{1-x}Ti_xSi_2O_9$ ceramic can be controlled to −5.1 ppm/°C by Ti^{4+} substitution for Sn^{4+} due to the appearance of $CaTiO_3$ (positive τ_f value) second phase [11]. $HfSiO_4$ and $ZrSiO_4$ ceramics [19,20] exhibit similar crystal structures and microwave dielectric properties. Hf^{4+} shows similar characteristics to Zr^{4+} in $MSiO_4$ (M = Hf, Zr). Therefore, Zr^{4+}, Hf^{4+} and Sn^{4+} ions exhibit similar ionic radii and valence states. $Ca_2ZrSi_4O_{12}$ belongs to the cyclosilicate class [21] and exhibits low-permittivity microwave dielectric properties [22]. Zr^{4+}, Hf^{4+} and Sn^{4+} ions could occupy the same site in $Ca_2MSi_4O_{12}$ (M = Zr, Hf and Sn). $Ca_2HfSi_4O_{12}$ could exhibit a similar crystal structure to that of $Ca_2ZrSi_4O_{12}$ and possess low-permittivity microwave dielectric properties due to the existing large number of Si–O bonds. However, the microwave dielectric properties of $Ca_2HfSi_4O_{12}$ have never been reported.

In this work, $Ca_2(Hf_{1-x}Sn_x)Si_4O_{12}$ ($0 \le x \le 0.5$) was prepared via the solid-state method. The τ_f value was adjusted to near zero by $CaSnSiO_5$ second phase with a positive τ_f value [23]. The correlation between the phase compositions and microwave dielectric properties of $Ca_2(Hf_{1-x}Sn_x)Si_4O_{12}$ ($0 \le x \le 0.5$) was investigated.

2. Experimental

In accordance with stoichiometry, SnO_2 (50–70 nm, 99.9 %), $CaCO_3$ (99.5 %), SiO_2 (99.5 %) and HfO_2 (99.5 %) powders were weighed to prepare $Ca_2(Hf_{1-x}Sn_x)Si_4O_{12}$ ($0 \le x \le 0.5$) ceramics by the solid-state method. The mixtures dispersed in deionised water were milled for 5 h

* Corresponding author at: School of Optical and Electronic Information, Huazhong University of Science and Technology, Wuhan, 430074, PR China.
E-mail address: wenlei@mail.hust.edu.cn (W. Lei).

https://doi.org/10.1016/j.materresbull.2020.110887
Received 19 April 2019; Received in revised form 20 February 2020; Accepted 10 April 2020
Available online 18 April 2020
0025-5408/

Table 1
Microwave dielectric properties of some typical silicates oxide.

Ceramics	S.T. (°C)	ε_r	$Q\times f$ (GHz)	τ_f (ppm/°C)	Reference
$(Zn_{0.95}Co_{0.05})_2SiO_4$	1200	6.5	57,000	−55.0	[7]
Mg_2SiO_4	1450	7.5	112,780	−63.0	[8]
$BaSiO_3$	1200	11.1	6,600	−35.0	[9]
$Ca_3SnSi_2O_9$	1500	8.4	92,000	−60.0	[10]
$Ca_3HfSi_2O_9$	1375	10.3	45,000	−46.9	[11]
$Ca_3ZrSi_2O_9$	1400	10.6	54,800	−76.8	[12]
$CaMgSiO_4$	1350	7.1	62,500	−62.9	[13]
$CaMgSi_2O_6$	1250	7.8	67,100	−24.1	[14]
$Ca_2ZnSi_2O_7$	1300	11.0	13,500	−64.3	[15]

using a planetary milling machine (QM-3SP2, Zhenguang, Nanjing, China). After drying at 80 °C for 10 h, the raw materials were calcined at 1150 °C for 5 h with a heat rate 5 °C/min. After remilling for 5 h and drying again, the fine powders with 5 wt% PVA solution were uniaxially pressed into samples with dimension of 12 mm in diameter and 6 mm in height under a pressure of 150 MPa. Finally, the samples were sintered at temperatures of 1350 °C – 1375 °C for 5 h with a heating rate of 5 °C/min in air.

The bulk densities (ρ_{obs}) of the sintered sample were measured by using the Archimedes method. The relative density (ρ_{rel}) was calculated using the following formula [24]:

$$\rho_{rel} = \frac{\rho_{obs}}{\rho_{the}} \tag{1}$$

Where ρ_{the} is the theoretical density from the X-ray diffraction (XRD) refinement data.

For multiphase composite ceramics, ρ_{rel} can be calculated by

$$\rho_{the} = \frac{W_1 + W_2}{W_1/\rho_1 + W_2/\rho_2} \tag{2}$$

Where W_1, W_2, ρ_1 and ρ_2 are the weight percentages from the weight fraction (W) and the theoretical densities from the XRD refinement data of phases 1 and 2, respectively.

Room-temperature powder XRD with CuK_α radiation (XRD–7000, Shimadzu, Kyoto, Japan) was utilised to analyse the phase compositions. Further phase analysis and evolution of crystal structure were performed by Rietveld refinement [25–27]. The microstructures of the thermally etched samples were observed by scanning electron microscopy (SEM, Sirion 200, the Netherlands). The temperature of the thermally etched samples was 75 °C below the densification temperatures for 30 min.

The microwave dielectric properties were evaluated at 11–13 GHz using a network analyser (Agilent E8362B, Agilent Technologies, USA). The $Q\times f$ value was measured using the Hakki–Coleman method [28]. ε_r and τ_f values were measured by using parallel silver boards. The τ_f value was calculated by

$$\tau_f = \frac{1}{f(T_0)}\frac{[f(T_1) - f(T_0)]}{T_1 - T_0} \tag{3}$$

Where $f(T_1)$ and $f(T_0)$ represent the resonant frequencies at T_1 (85 °C) and T_0 (20 °C), respectively.

3. Results and discussion

Fig. 1 shows the XRD patterns of $Ca_2(Hf_{1-x}Sn_x)Si_4O_{12}$ ($0 \le x \le 0.5$) ceramics sintered at densification temperature. $Ca_2(Hf_{1-x}Sn_x)Si_4O_{12}$ ($0 \le x \le 0.2$) exhibited a $Ca_2HfSi_4O_{12}$ single phase (JCPDS No. 50-0301). When $x = 0.25$, the Sn^{4+} could not completely replace Hf^{4+} at $(Hf_{1-x}Sn_x)^{4+}$ site, and the second phase $CaSnSiO_5$ appeared. As the Sn content increased in $Ca_2(Hf_{1-x}Sn_x)Si_4O_{12}$, the XRD intensity of the $CaSnSiO_5$ (JCPDS No. 86-0928) phase enhanced gradually, and the other $CaSiO_3$ (JCPDS No. 074-0874) second phase was observed at $x \ge 0.3$. The coexistence of $Ca_2HfSi_4O_{12}$, $CaSnSiO_5$, and $CaSiO_3$ phases was achieved at $Ca_2(Hf_{1-x}Sn_x)Si_4O_{12}$ ($0.3 \le x \le 0.5$). This result showed that the maximum solubility of $Ca_2(Hf_{1-x}Sn_x)Si_4O_{12}$ was between 0.2 and 0.25.

Fig. 2 shows the refined XRD pattern and the crystal structure of the $Ca_2HfSi_4O_{12}$ ceramic. $Ca_2HfSi_4O_{12}$ belongs to cyclosilicate class, the $[SiO_4]$ tetrahedra rings of which were connected by $[HfO_6]$ octahedron. The weight R-factor R_{wp}, profile R-factor R_p, goodness-of-fit indicator χ^2 values and lattice parameters of $Ca_2(Hf_{1-x}Sn_x)Si_4O_{12}$ ($0 \le x \le 0.25$) ceramics are listed in Table 2. In Fig. 2a, the observed diffraction profiles were consistent with the calculated result, although a minimal mismatch of the refined XRD pattern was observed at low angles due to the difficulties in modelling the diffraction peak asymmetry. The Rietveld discrepancy factors confirmed that the results of Rietveld refinement were reliable. The lattice parameters of $Ca_2(Hf_{1-x}Sn_x)Si_4O_{12}$ decreased linearly when x changed from 0 to 0.2, which corresponded to the reduction in ionic radius (r_{Hf}^{4+} = 0.710 Å, r_{Sn}^{4+} = 0.690 Å) [29].

The SEM micrographs of the thermally etched $Ca_2(Hf_{1-x}Sn_x)Si_4O_{12}$ ($0 \le x \le 0.5$) ceramics were observed in Fig. 3. The images display dense microstructures. In Fig. 3a and b, no different grains could be observed, and the average grain size presented a reducing tendency. The grain of $Ca_2(Hf_{1-x}Sn_x)Si_4O_{12}$ became uniform by Sn^{4+} substitution for Hf^{4+}. The average grain sizes of the $Ca_2HfSi_4O_{12}$ single phase and $Ca_2(Hf_{1-x}Sn_x)Si_4O_{12}$ ($x = 0.2$) ceramics were approximately 9 (Fig. 3a) and 3 (Fig. 3b) μm, respectively. The $CaSiO_3$ liquid phase appears in Fig. 3d–f. The grain shape of the $CaSiO_3$ ceramic was lost and the glass phase existed on its surface because of its narrow sintering temperature range [30]. As the x value increased in $Ca_2(Hf_{1-x}Sn_x)Si_4O_{12}$ ($0.3 \le x \le 0.5$) ceramics, the amount of the $CaSiO_3$ and $CaSnSiO_5$ second phase increased gradually. No obvious $CaSiO_3$ second phase was observed in $Ca_2(Hf_{0.75}Sn_{0.25})Si_4O_{12}$ (Fig. 3c), which agreed with Fig. 1 and Table 2.

The variation tendency of ε_r value, ionic polarizability of $(Hf_{1-x}Sn_x)^{4+}$ and relative density with x are shown in Fig. 4. A high relative density (approximately 98 %) was obtained in the single-phase area. With increasing x value in the $Ca_2(Hf_{1-x}Sn_x)Si_4O_{12}$ ($0.25 \le x \le 0.5$), the relative density of multiphase ceramics presented a reducing tendency because of the increasing amount of $CaSiO_3$ (with a relative density of 87.2 %) [31]. In the single-phase area, the ε_r value showed a linearly reducing tendency with x changing from 0 to 0.2, the variation of which was similar to that of the ionic polarizability of $(Hf_{1-x}Sn_x)^{4+}$ [32]. As the x increased, the total polarizability and the theoretical relative permittivity of $Ca_2(Hf_{1-x}Sn_x)Si_4O_{12}$ could decrease according to Clausius-Mossotti equation. The variation tendency of relative density exhibited a difference from that of the ε_r value. As a result, the variation tendency of the ε_r value was dominated by the ionic polarizability of $(Hf_{1-x}Sn_x)^{4+}$ rather than the relative density in the single-phase area. In the multiphase area ($0.25 \le x \le 0.3$), the ε_r was mainly affected by the second phase and the ε_r value of $Ca_2(Hf_{1-x}Sn_x)Si_4O_{12}$ ceramics demonstrated an increasing tendency because of the appearance of the $CaSnSiO_5$ phase (ε_r = 11.4) [31]. As the Sn content increased ($0.4 \le x \le 0.5$), the ε_r value exhibited a reducing tendency due to the increasing amount of $CaSiO_3$ second phase (ε_r = 6.9) [31]. The appearance of $CaSiO_3$ second phase with the lower ε_r and ρ_{rel} values could deteriorate the ε_r and ρ_{rel} of $Ca_2(Hf_{1-x}Sn_x)Si_4O_{12}$ even if the content of $CaSnSiO_5$ second phase with the higher ε_r and ρ_{rel} values increased. So, the ε_r of $Ca_2(Hf_{1-x}Sn_x)Si_4O_{12}$ ($0.4 \le x \le 0.5$) ceramics was affected by second phase and the relative density.

Fig. 5 shows the $Q\times f$ and τ_f values of $Ca_2(Hf_{1-x}Sn_x)Si_4O_{12}$ ($0 \le x \le 0.5$) ceramics with changing x value. The $Q\times f$ value exhibited an opposite variation trend from τ_f values. When $x = 0.2$, the maximum $Q\times f$ value ($Q\times f$ = 49,500 GHz) was obtained. When x changed from 0 to 0.2, the $Q\times f$ value of the $Ca_2(Hf_{1-x}Sn_x)Si_4O_{12}$ ($0 \le x \le 0.2$) ceramics increased linearly in the single-phase area. According to the report of Song [11], the relative covalence of Sn-O is larger than that of Hf-O, and the $Q\times f$ value is related to the relative covalence of $Hf_{1-x}Sn_x$ site. The large relative covalence of $Hf_{1-x}Sn_x$ site corresponded to a higher

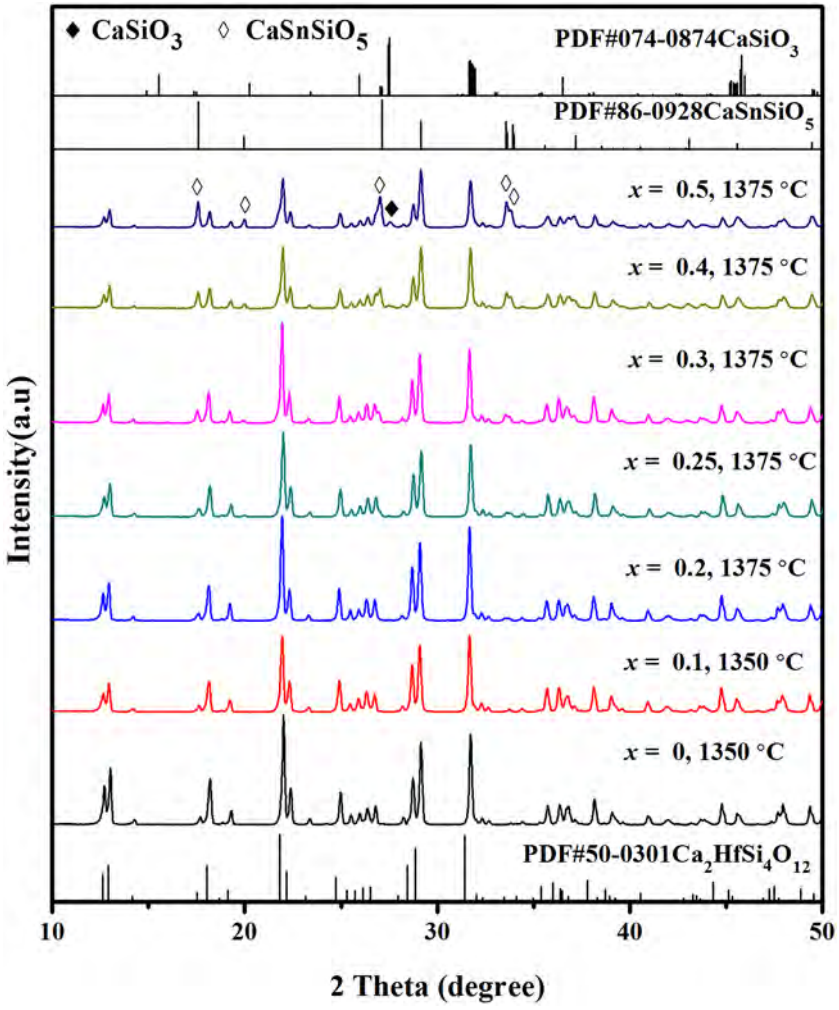

Fig. 1. XRD patterns of $Ca_2(Hf_{1-x}Sn_x)Si_4O_{12}$ ($0 \le x \le 0.5$) ceramics sintered at their densification temperature.

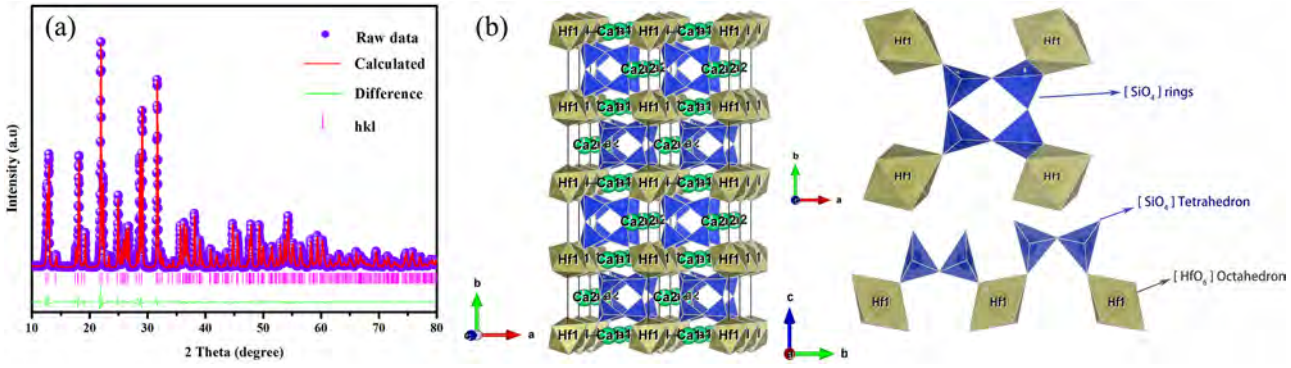

Fig. 2. (a) Rietveld refinement of the XRD pattern for the $Ca_2HfSi_4O_{12}$ ceramics sintered at densification temperature, (b) crystal structure of $Ca_2HfSi_4O_{12}$.

Table 2
The weight percentage of second phase, lattice parameters, and Rietveld discrepany factors of $Ca_2(Hf_{1-x}Sn_x)Si_4O_{12}$ ($0 \le x \le 0.25$) ceramics sintered at their densification temperature.

x value	Second phase (*wt* %)	a (Å)	b (Å)	c (Å)	β (°)	V (Å^3)	R_{wp} (%)	R_p (%)	χ^2
0	–	7.408	13.688	5.327	108.828	511.267	7.32	4.99	6.6
0.1	–	7.397	13.672	5.323	108.819	509.390	6.75	4.89	5.9
0.2	–	7.388	13.661	5.319	108.795	508.170	7.36	5.26	6.2
0.25	$CaSnSiO_5$ (4.2%)	7.390	13.665	5.321	108.813	508.670	7.86	5.75	7.5

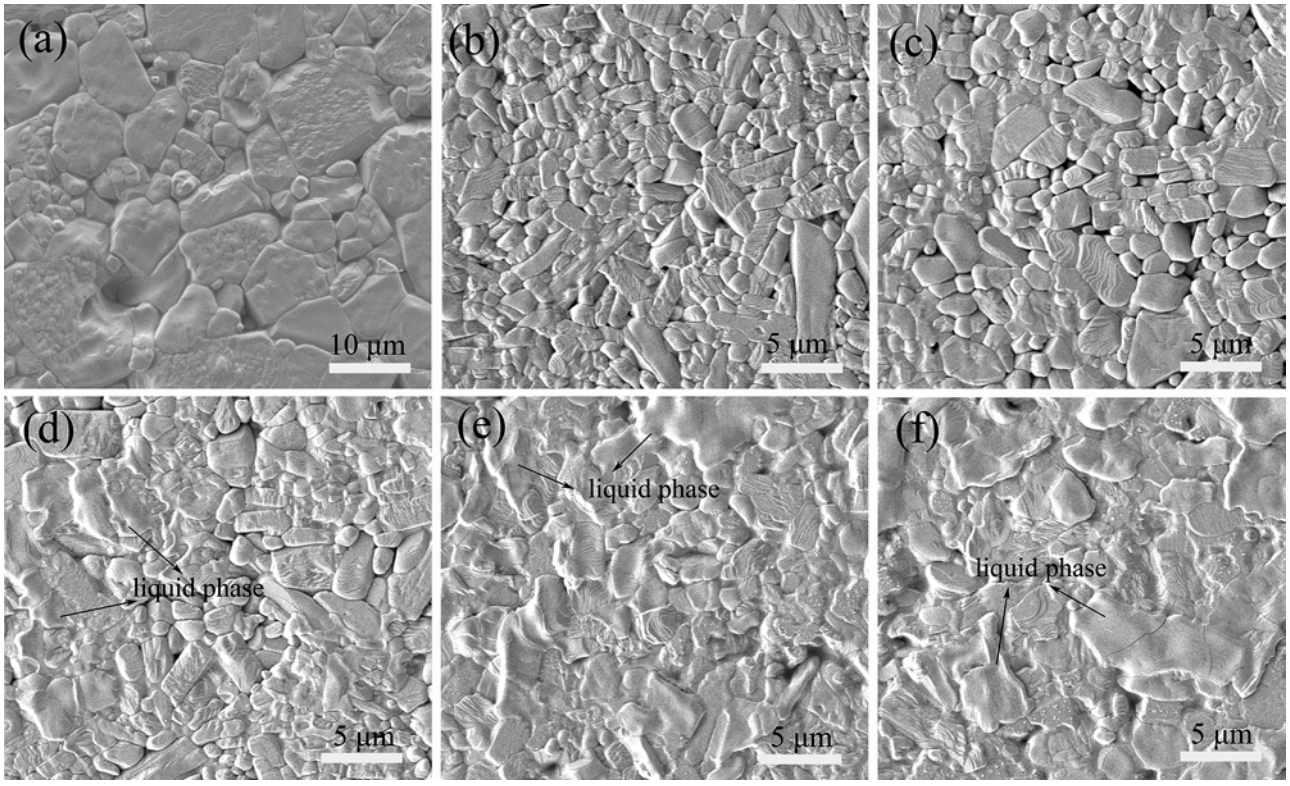

Fig. 3. SEM photographs of thermally etched $Ca_2(Hf_{1-x}Sn_x)Si_4O_{12}$ ($0 \le x \le 0.5$) ceramics sintered at different densification temperature: (a) $x = 0$, 1350 °C; (b) $x = 0.2$, 1375 °C; (c) $x = 0.25$, 1375 °C; (d) $x = 0.3$, 1375 °C; (e) $x = 0.4$, 1375 °C; (f) $x = 0.5$, 1375 °C.

$Q \times f$ value. The $Q \times f$ value was generally influenced by intrinsic and extrinsic factors [33]. Partial substitution of Sn^{4+} for Hf^{4+} at the $Hf_{1-x}Sn_x$ site could change the lattice vibrational modes of $Ca_2(Hf_{1-x}Sn_x)Si_4O_{12}$. Therefore, the $Q \times f$ value of the single-phase area was mainly affected by the intrinsic factors. In the multiphase area, with increasing amounts of $CaSnSiO_5$ and $CaSiO_3$ second phase, the $Q \times f$ value of the $Ca_2(Hf_{1-x}Sn_x)Si_4O_{12}$ ($0.25 \le x \le 0.5$) ceramics decreased linearly due to the negative effect of the second phase with a low $Q \times f$ value [31].

Fig. 5 shows that with the Sn^{4+} substitution for Hf^{4+}, the τ_f value of $Ca_2(Hf_{1-x}Sn_x)Si_4O_{12}$ ceramics in the single-phase area depicted a reducing tendency. In the multiphase area, the $CaSnSiO_5$ and $CaSiO_3$ second phase appeared, and the τ_f value of $Ca_2(Hf_{1-x}Sn_x)Si_4O_{12}$ ceramics was closely related to the phase compositions. The $CaSnSiO_5$ ceramic ($\tau_f = +62.5$ ppm/°C) possessed an abnormally positive τ_f value [23]. The τ_f value of the $Ca_2(Hf_{1-x}Sn_x)Si_4O_{12}$ ceramic could be controlled to near zero by $CaSnSiO_5$ phase at $x = 0.4$ ($\tau_f = -7.2$ ppm/°C) and $x = 0.5$ ($\tau_f = +1.6$ ppm/°C).

4. Conclusions

$Ca_2(Hf_{1-x}Sn_x)Si_4O_{12}$ ($0 \le x \le 0.5$) ceramics with low-permittivity microwave dielectrics properties were investigated sintered at

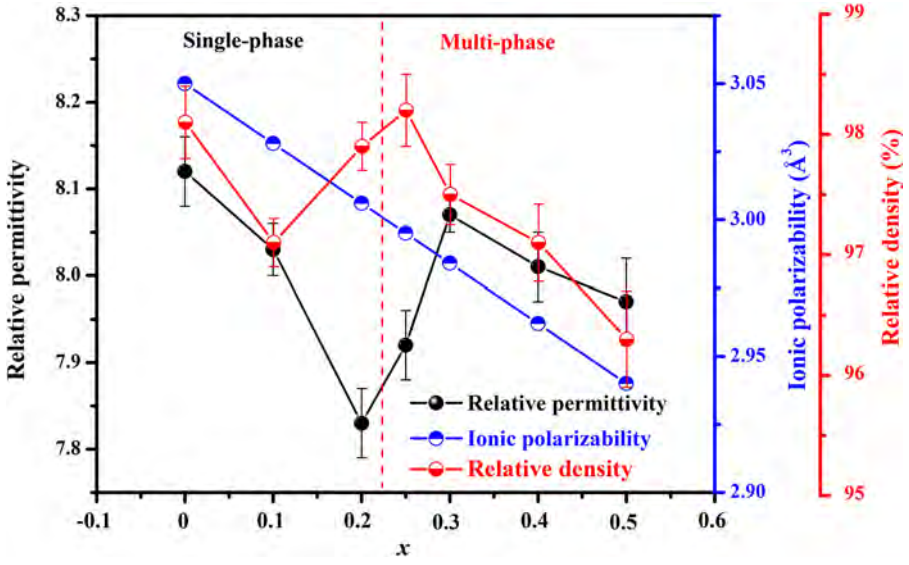

Fig. 4. The variation of relative permittivity, the ionic polarizability of $(Hf_{1-x}Sn_x)^{4+}$, and relative density with x value.

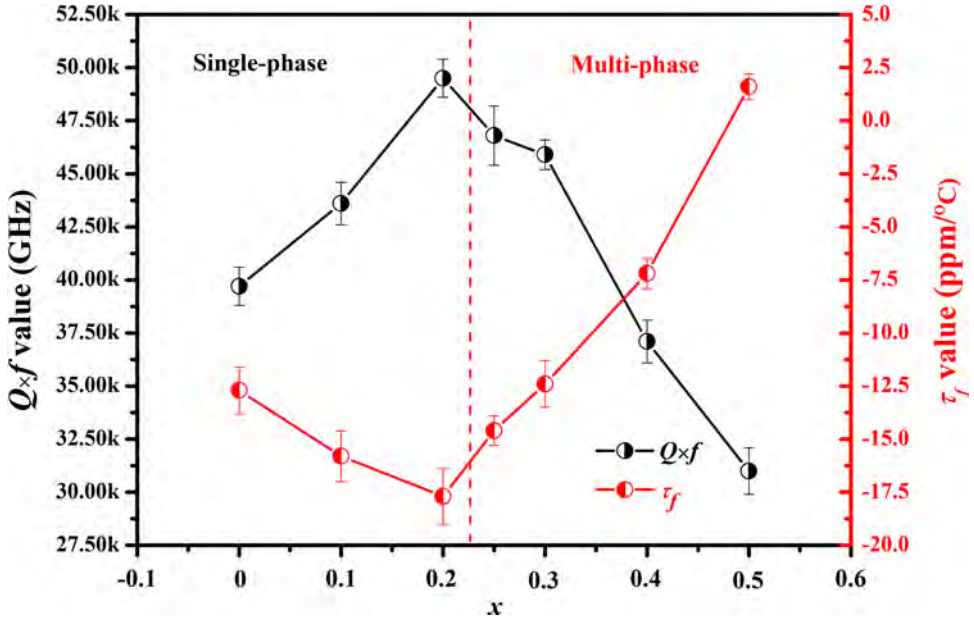

Fig. 5. The variation of $Q\times f$ and τ_f values of $Ca_2(Hf_{1-x}Sn_x)Si_4O_{12}$ ($0 \le x \le 0.5$) ceramics with x value.

1350 °C – 1375 °C for 5 h by the solid-state reaction method. Single-phase ceramics were obtained at $Ca_2(Hf_{1-x}Sn_x)Si_4O_{12}$ ($0 \le x \le 0.2$). The partial Sn^{4+} substitution of Hf^{4+} could decrease the ε_r and τ_f values and improve the $Q\times f$ value of $Ca_2(Hf_{1-x}Sn_x)Si_4O_{12}$ ceramics. When $x = 0.20$, the sample exhibited the maximum $Q\times f$ value ($Q\times f$ = 49,500 GHz). However, the $CaSnSiO_5$ and $CaSiO_3$ second phase appeared at $Ca_2(Hf_{1-x}Sn_x)Si_4O_{12}$ ($0.25 \le x \le 0.5$). The $Q\times f$ value showed a reducing trend, and the τ_f value could be controlled to near zero by the $CaSnSiO_5$ phase. Good microwave dielectric properties (ε_r = 8.0, $Q\times f$ = 37,100 GHz, $\tau_f = -7.2$ ppm/°C) could be achieved in the $Ca_2(Hf_{1-x}Sn_x)Si_4O_{12}$ ($x = 0.4$) sintered at 1375 °C.

CRediT authorship contribution statement

Kang Du: Writing - original draft, Data curation. **Xiao-Qiang Song:** Software, Formal analysis. **Zheng-Yu Zou:** Supervision, Validation. **Jun Fan:** Investigation, Methodology. **Wen-Zhong Lu:** Conceptualization, Methodology. **Wen Lei:** Writing - review & editing.

Declaration of Competing Interest

The authors declare that they have no known competing financial interests or personal relationships that could have appeared to influence the work reported in this paper.

Acknowledgements

This work was supported by the National Natural Science Foundation of China (NSFC-51572093 and 51772107), Research Projects of Electronic Components and Devices of China (1807WM0004), and the Major Programs of Technical Innovation in Hubei Province of China (2018AAA039). The authors are grateful to the Analytical and Testing Center, Huazhong University of Science and Technology, for SEM analyses.

References

[1] T.A. Vanderah, Talking ceramics, Science 298 (2002) 1182–1184.
[2] T. Tsunooka, M. Androu, Y. Higashida, H. Sugiura, H. Ohsato, Effect of TiO_2 on sinterability and dielectric properties of high-Q forsterite ceramics, J. Eur. Ceram. Soc. 23 (2003) 2573–2578.
[3] I.M. Reaney, D. Iddles, Microwave dielectric ceramics for resonators and filters in mobile phone networks, J. Am. Ceram. Soc. 89 (2006) 2063–2072.
[4] K.X. Song, Y.Q. Yang, P. Zheng, J.M. Xu, H.B. Qin, Microstructures and microwave dielectric properties of $(Mg_{1-x}Sr_x)_2Al_4Si_5O_{18}$ ceramics, J. Inorg. Mater. 27 (2012) 575–579.
[5] H.W. Chen, H. Su, H.W. Zhang, T.C. Zhou, B.W. Zhang, J.F. Zhang, X.L. Tang, Low-temperature sintering and microwave dielectric properties of $(Zn_{1-x}Co_x)_2SiO_4$ ceramics, Ceram. Int. 40 (2014) 14655–14659.
[6] J. Xi, B.B. Lu, J.J. Chen, G.H. Chen, F. Shang, J.W. Xu, C.R. Zhou, C.L. Yuan, Ultralow sintering temperature and permittivity with excellent thermal stability in novel borate glass-ceramics, J. Non-Crystal. Solids 521 (2019) 119527.
[7] D.H. Jiang, J.J. Chen, B.B. Lu, J. Xi, F. Shang, J.W. Xu, G.H. Chen, Preparation, crystallization kinetics and microwave dielectric properties of CaO-ZnO-B_2O_3-P_2O_5-TiO_2 glass-ceramics, Ceram. Int. 45 (2019) 8233–8237.
[8] K.X. Song, X.M. Chen, C.W. Zheng, Microwave dielectric characteristics of ceramics in Mg_2SiO_4–Zn_2SiO_4, system, Ceram. Int. 34 (2008) 917–920.
[9] W. Lei, Z.Y. Zou, Z.H. Chen, B. Ullah, A. Zeb, X.K. Lan, W.Z. Lu, G.F. Fan, X.H. Wang, X.C. Wang, Controllable τ_f value of barium silicate microwave dielectric ceramics with different Ba/Si ratios, J. Am. Ceram. Soc. 101 (2017) 25–30.
[10] S.P. Wu, D.F. Chen, Y.X. Mei, Q. Ma, Synthesis and microwave dielectric properties of $Ca_3SnSi_2O_9$ ceramics, J. Alloys. Compd. 521 (2012) 8–11.
[11] X.Q. Song, K. Du, X.Z. Z, J. Li, W.Z. Lu, X.C. Wang, W. Lei, Crystal structure, phase composition and microwave dielectric properties of $Ca_3MSi_2O_9$ ceramics, J. Alloys. Compd. 750 (2018) 996–1002.
[12] A. Kan, H. Ogawa, H. Ohsato, Synthesis and crystal structure–microwave Dielectric property relations in Sn-substituted $Ca_3(Zr_{1-x}Sn_x)Si_2O_9$ solid solutions with cuspidine structure, J. Appl. Phys. 46 (2007) 7108–7111.
[13] H.F. Zhou, J. Huang, X.H. Tan, G.C. Fan, X.L. Chen, H. Ruan, Microwave dielectric properties of low-permittivity $CaMgSiO_4$ ceramic, J. Mater. Sci. – Mater. Electron. 28 (2017) 15258–15262.
[14] J. Zhang, Y.Y. Zhou, Z.X. Yue, Low-temperature sintering and microwave dielectric properties of LiF-doped $CaMg_{1-x}Zn_xSi_2O_6$ ceramics, Ceram. Int. 39 (2013) 2051–2058.
[15] T. Joseph, M.T. Sebastian, Microwave dielectric properties of $(Sr1\text{-}xAx)_2(Zn_{1-x}B_x)Si_2O_7$ ceramics (A = Ca, Ba and B = Co, Mg, Mn, Ni), J. Am. Ceram. Soc. 93 (2010) 147–154.
[16] S.P. Wu, C. Jiang, Y.X. Mei, W.P. Tu, Synthesis and microwave dielectric properties of Sm_2SiO_5 ceramics, J. Am. Ceram. Soc. 95 (2012) 37–40.
[17] M.T. Sebastian, R. Ubic, H. Jantunen, Low-loss dielectric ceramic materials and their properties, Inter. Mater. Reviews. 60 (2015) 392–412.
[18] I.M. Reaney, D. Iddles, Microwave dielectric ceramics for resonators and filters in mobile phone networks, J. Am. Ceram. Soc. 89 (2010) 2063–2072.
[19] J. Varghese, T. Joseph, K.P. Surendran, T.P.D. Rajan, M.T. Sebastian, Hafnium silicate: a new microwave dielectric ceramic with low thermal expansivity, Dalton Trans. 44 (2015) 5146–5152.
[20] J. Varghese, T. Joseph, M.T. Sebastian, $ZrSiO_4$ ceramics for microwave integrated circuit applications, Mater. Lett. 65 (2011) 1092–1094.
[21] S. Colin, B. Dupre, G. Venturini, B. Malaman, C. Gleitzer, Crystal structure and infrared spectrum of the cyclosilicate $Ca_2ZrSi_4O_{12}$, J. Solid State Chem. 102 (1) (1993) 242–249.
[22] P.G. Shakhil, Albin. Antoney, P.V. Narayanan, T. Sanaj, Lijin. Jose, N.S. Arun, R. Ratheesh, Preparation, characterization and dielectric properties of $Ca_2ZrSi_4O_{12}$ ceramic and filled silicone rubber composites for microwave circuit applications, Mater. Sci. Eng-B 255 (2017) 115–121.

[23] S.P. Wu, D.F. Chen, C. Jiang, Y.X. Mei, Q. Ma, Synthesis of monoclinic $CaSnSiO_5$, ceramics and their microwave dielectric properties, Mater. Lett. 91 (2013) 239–241.
[24] S. Lei, H. Fan, X. Ren, J. Fang, L. Ma, H. Tian, Microstructure, phase evolution and interfacial effects in a new $Zn_{0.9}Mg_{0.1}TiO_3$-$ZnNb_2O_6$ ceramic system with greatly induced improvement in microwave dielectric properties, Scripta Mater. 146 (2018) 154–159.
[25] H.M. Rietveld, A profile refinement method for nuclear and magnetic structures, J. Appl. Cryst. 2 (1969) 65–71.
[26] A.C. Larson, R.B. Von Dreele, Los Alamos National Laboratory Report, LAUR, 199486-199748.
[27] B.H. Toby, EXPGUI, a graphical user interface for GSAS, J. Appl. Cryst. 34 (2001) 210–213.
[28] B.W. Hakki, P.D. Coleman, A dielectric resonant method of measuring inductive capacitance in the millimeter range, IRE Trans. Microwave Theory Technol. 8 (1960) 402–410.
[29] R.D. Shannon, Revised effective ionic radii and systematic studies of interatomic distances in halides and chalcogenides, Acta Crystallogr. A 32 (1976) 751–767.
[30] R.P. Sreekanth Chakradhar, B.M. Nagabhushana, G.T. Chandrappa, K.P. Ramesh, J.L. Rao, Solution combustion derived nanocrystalline macroporous wollastonite ceramics, Mater. Chem. Phys. 95 (2006) 169–175.
[31] K. Du, X.Q. Song, J. Li, J.M. Wu, W.Z. Lu, X.C. Wang, W. Lei, Optimized phase compositions and improved microwave dielectric properties based on calcium tin silicates, J. Eur. Ceram. Soc. 39 (2019) 340–345.
[32] R.D. Shannon, Dielectric polarizabilities of ions in oxides and fluorides, J. Appl. Phys. 73 (1993) 348–366.
[33] W. Lei, A. Ran, X.C. Wang, W.Z. Lu, Phase evolution and near-zero shrinkage in $BaAl_2Si_2O_8$ low-permittivity microwave dielectric ceramics, Mater. Res. Bull. 50 (2014) 235–239.